Civil and Environmental Engineering
Vol. 0, Issue 0, DOI: 10.2478/cee-2026-0081

Effects of Geogrid Reinforcement and Tire Contact Pressure on Responses of Flexible Pavement over Weak Subgrade

Nawal D. SALMAN[1,*], Hasan H. JONI[1]

[1] College of Civil Engineering, University of Technology, Baghdad, Iraq.

* corresponding author: Nawal.D.Salman@uotechnology.edu.iq

Date of Submission: 08 November 2025
Revision Date: 08 December 2025
Date of Acceptance: 17 December 2025

Civil and Environmental Engineering
Journal of the Faculty of Civil Engineering | University of Žilina

Abstract

Flexible pavements constructed over weak subgrades with a California Bearing Ratio (CBR) range of 2-4 % are subjected to premature failure owing to excessive stress and deformation. Their performance is significantly influenced by the actual contact tire pressure. These problems can be addressed using geogrid reinforcement. In this study, the impact of tire contact pressure on geogrid-reinforced flexible pavements built over weak subgrades was examined using physical models with a (1/3) scale. Five pavement sections were tested: control (unreinforced), which consists of three layers wearing asphalt layer of 5 cm, a bituminous base of 6 cm, subbase layer of 9 cm, all resting on a weak subgrade of clay soil of 50 cm. The reinforced sections were biaxial and triaxial geogrid reinforcement at the subbase-subgrade interface, and at the middle of the subbase course layer. Repeated axle loads were applied at three directly measured tire contact pressures (480, 560, and 690 kPa). Vertical stresses were measured at the bottom of the asphalt layer and the top of the subgrade. Increasing the tire pressure from 480 to 690 kPa raised the vertical stresses at the asphalt bottom by 67% in the control section and by 56% in the reinforced sections. At the top of the subgrade, the same increase resulted in vertical stress rises of 42 % for the control section and 32 % for the reinforced sections. Geogrid reinforcement reduced vertical stress at high pressures effectively, with subbase-subgrade reinforcement showing better performance than reinforcement at the middle depth of subbase. However, reinforcement with a triaxial geogrid presented good performance under different tire contact pressures. where the geogrid reduces stresses at the bottom of the asphalt layer by 28% and 23% for the biaxial and triaxial geogrids, respectively, when used at the subbase-subgrade interface, while the geogrid reduces stresses at the top of the subgrade layer by 49% and 43% for the biaxial and triaxial geogrids, respectively. The results revealed that tire pressure is a fundamental factor that affects flexible pavement performance, especially when built over weak subgrades, whereas geogrid reinforcement could further contribute to better performance.

Keywords

Tire Contact Pressure; Flexible Pavement; Biaxial Geogrid; Triaxial Geogrid; Pavement Reinforcement.

1. Introduction

Flexible pavements are frequently utilized in highway building because of their easier construction, reduced initial costs, and comparatively low maintenance needs compared to rigid pavements or semi-rigid pavements. The asphalt surface (wearing course), base, subbase, and subgrade are the usual layers that comprise these pavements. The distribution of traffic loads from the surface to the subgrade is the main purpose of this layered structure. Nonetheless, the strength of

the subgrade and the system's capacity to disperse stresses efficiently are key factors in the performance of flexible pavements. These pavements are susceptible to early failures such as rutting, cracking, and excessive settlement when constructed on weak subgrades (Tasnim et al.,2021; Albayati & Al-Mosawe, H., 2023; Akram, H. A., 2022; Alhelyani, A., & Zhang, S., 2023), although asphalt pavements are prone to rutting even in the case of sufficiently bearable subgrades, where ruts can form only in asphalt mixtures. Geosynthetic materials like geotextiles and geogrids are frequently used in pavement constructions to overcome these issues (Jasim A.F. et al., 2021; Al-Qadi I.L., 2005; Jebur, F.F. et al., 2021; Jayalath et al.,2018). These reinforcements increase pavement service life, improve load distribution, and reduce deformation. For example, research documented that a 9.8 Traffic Benefit Ratio (TRB) could be achieved when geogrid reinforcement is placed at the optimum position (Zadehmohamad et al., 2022). The system's structural integrity can be enhanced by installing geosynthetics at a variety of interfaces, such as between the base and subgrade, between the base and subbase, or even inside the granular base layer within the upper third (Al-Qadi I.L., 2005; Jayalath G. et al.,2018; Nazal M.D., 2007; Abu-Farsakh M. &Nazzal M., 2009; Ibrahim S. et al., 2016). It has been demonstrated that reinforced pavements reduce the subgrade's stress, which minimizes the subgrade failure potential (Zornberg J.G., 2016).

Lateral restraint, enhanced bearing capacity, the tension membrane effect, and separation are the mechanisms by which geosynthetics' reinforcing effect works. The literature has provided a thorough description of these processes (Zornberg J.G., 2016; Cuelho E.V. & Perkins S.W., 2017; Alimohammadi H. et al., 2021; Jayalath G. et al., 2021), where incorporating geogrid within the pavement layer can improve load distribution through interlocking with aggregate of base or subbase layer that produces lateral confinement and reduces stresses transmitted to subgrade (Kwon & Tutumluer, 2009). However, the mechanical properties of the geogrid, such as tensile strength, stiffness, type of geogrid and opening shape, and subgrade strength, play a significant role in reinforcement and could affect the percent of improvement. numerical and experimental studies validate these findings (Wimalasena & Jayalath, 2020). In addition, the numerous geogrids available and their various forms and properties make it difficult for researchers to cover all of these types; thus, this topic is still subject to ongoing research.

The amount and distribution of stresses applied to pavement systems are also controlled by tire pressure. The contact area is decreased by higher tire pressures, increasing the vertical contact stresses. Particularly in the asphalt surface and subgrade layers, these pressures accelerate rutting and fatigue (Al-Qadi I.L. & Wang H., 2011). According to (Roberts et al.,1986), actual tire pressures in use are frequently higher than those predicted during design, which leads to increased tensile stresses and quicker degradation of thin flexible pavements. Although this observation may have been made long ago, recent study has indicated that tire contact pressures remain problematic for pavement performance, even with the current technology of modern tire types, which confirmed that contact pressures impact pavement life through their effects on fatigue cracking and permanent deformation (Rahman et al.,2025). (Marshek et al., 1986; Rahman et al.,2025) discovered that tire pressure dramatically raises tensile strains and compressive stress inside the asphalt layer, whereas axle load largely affects rutting and subgrade strain. Tires that are overinflated concentrate stresses beneath the tire's centreline, increasing the risk of subgrade failure. Furthermore, experimental research conducted by (Bonaquist et al.,1990) showed that fatigue damage equivalent to adding 2,000 pounds (907 kg) of axle load was caused by raising contact tire pressure from 76 psi (524 kPa) to 140 psi (965 kPa). According to Sebaaly and Tabatabaee (1989), the usage of wide-base radial tires resulted in the most severe strain responses in thin asphalt layers.

Although tire pressure effects and geosynthetic reinforcement have been the subject of several studies, limited studies have examined their combined impact, especially in scaled physical models of flexible pavements over weak subgrades. Understanding this interaction is significant for optimizing pavement design under increasingly variable loading conditions. This study is designed to examine the structural response of scaled models of flexible pavements reinforced with geogrid under weak subgrade conditions and different tire pressures. Laboratory flexible pavement models were prepared in a metal box with specific layer thickness and geogrid reinforcement at the middle of the subbase layer and at the subbase-subgrade interface each pavement section was subjected to repeated wheel load at 45 °C ± 2 °C temperature of pavement. The particular goal is to model various tire pressure levels (480, 560, and 690 kPa), which correspond to low, moderate, and

high pressure, and evaluate how they affect pavement compressive vertical stress at the top of the subgrade and vertical stress at the bottom of the asphalt layer for direct comparison between unreinforced and reinforced sections.

2. Materials and Methodology

2.1. Methodology Background

Previous research adopted accelerated load test and an instrumented test box in their studies as effective testing methodologies for pavement response monitoring. Based on these methods, this study utilizes a control laboratory accelerated loading setup to evaluate geogrid reinforcement and tire contact pressure effects on the response of flexible pavement at high temperature (45 ± 2) °C.

2.2. Subgrade Soil

The subgrade soil was clay soil brought from a construction site in Baghdad city. The Unified Soil Classification System (USCS) classifies it as a lean clay soil with low plasticity (CL) with a low plasticity index of 23.36% and a liquid limit of 42.86%. The AASHTO classifies it as an A-7 soil with a group index of 88.2. As shown in Table 1, the optimum moisture content was 16.8% and the specific gravity (Gs) was determined to be 2.690. The optimum moisture content (OMC) of soil is determined through conducting a series of standard compaction tests on a soil sample at different moisture contents. each sample is compacted in a standard mold placed in three layers. Each layer received 25 blows. A dry unit weight of each sample was calculated after oven drying of the samples and plotting against moisture content levels, the peak point of the compaction curves, which corresponds to the maximum dry unit weight, is identified as the optimum moisture content (OMC). During the testing procedure, the subgrade soil index strength was characterized using the CBR test (ASTM D1833-07). Examining the unsoked CBR at various water contents was required in order to select the worst situations that lead to low CBR, which is where the lift's subgrade soil was placed (Decký et al., 2015). This was accomplished by creating and implementing a CBR (unsoaked) testing program. To develop weak subgrade soil, the moisture content was increased to a higher level. As a result, the soil was compacted at a level higher than the optimal water content of 26%, resulting in a CBR value of 2.1%, as seen in Figure 1.

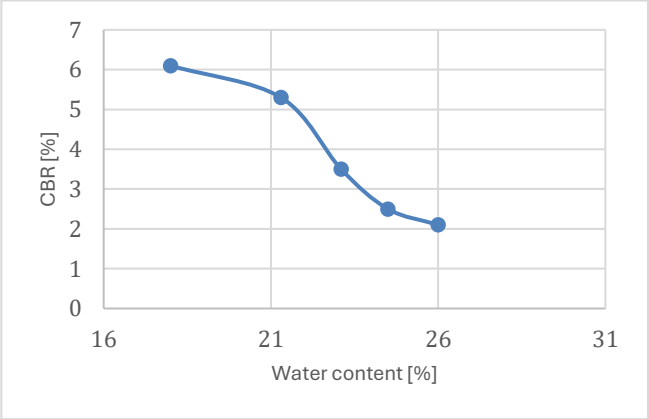

Figure 1: Differences in Soil CBR According to Moisture Content

2.3. Subbase Material

The sub-base, which is frequently utilized in the construction of flexible pavement, was acquired from the Al-Ubaidei asphalt plant. In accordance with the State Organization of Roads and Bridges' Standard Specification for Roads and Bridges (SCRB, 2003), standard laboratory tests were performed on subbase materials to ascertain their properties, such as sieve analysis, dry unit weight, and CBR ratio with compaction to 95% of the maximum dry density. Figure 2 displays the sub-base material's compaction curve, and Table 1 describes the material's mechanical and physical characteristics along with the

relevant requirements. According to the requirements, the subbase material was type B, and the subbase material's gradation is shown in Table 2.

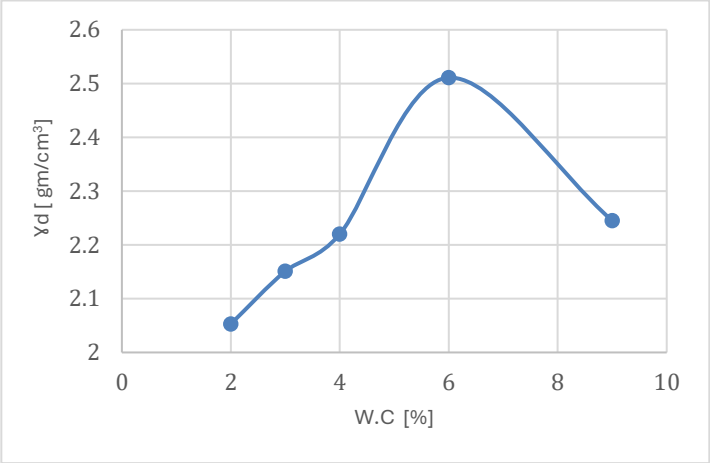

Figure 2: Subbase Standard Compaction Curve

2.3. Asphalt Binder

Al-Dura Refinery supplied a (40-50) penetration grade of asphalt binder, which was utilized to prepare the asphalt concrete mixture for the bituminous base and wearing surface course. The physical characteristics of the applied asphalt binder are shown in Table 3.

2.4. Base Course Material

Al-Ubaidei Asphalt Plant provided the aggregates for the base material. Table 2 displays the base course material gradation. As indicated in Table 4, a stabilized course with (40–50) grade asphalt was created using the Marshall design process, with an optimum asphalt content of 3.7%, air voids of 4.1%, and density of 2.311 kg/cm3.

Table 1: Physical and Mechanical Test for Subgrade and Subbase Material

Tests	Subgrade	Subbase	Specifications
Liquid Limit [%]	42.86	22	ASTM D 4318
Plastic Limit [%]	19.5	0	ASTM D 4318
Plasticity Index [%]	23.36	Na	ASTM D 4318
Specific gravity [-]	2.690	2.57	ASTM D -854-14
Maximum dry Density [g/cm^3]	1.75	2.50	ASTM D 1557-07
Optimum Moisture Content %	16.8	6 %	ASTM D 2216
CBR @ 95 [%] Compaction	8.2	35.10 %	ASTM D 1883
Classification of Soil	CL	GW-GM	USCS
Cu [-]		83.3	
Cc [-]		1.01	

Notes
Na: Not available
Cu: Coefficient of uniformity, Cc: Coefficient of curvature

Table 2: Iraqi Standards for wearing, Base, and Subbase coarse aggregate gradation [SCRB, 1983-R6]

Sieve Size [mm]	Sieve No. [inch]	Aggregate Material Gradation					
		Wearing Course		Base course		Subbase Course	
		Iraqi Standards Passing [%]	Blending [%]	Iraqi Standards Passing [%]	Blending [%]	Iraqi Standards Type B	Passing [%]
50.8	2	----	----	----	----	100	100
37.5	1.5			100	100	75-95	90.6
25	1			90-100	95	----	----
19	¾			76-90	83	----	----
12.5	½	100	100	56-80	68	----	----
9.5	3/8	80-100	88	48-74	61	40-75	57.5
4.75	No. 4	46-76	60	29-59	44	30-60	41.5
2.36	No. 8	28-58	41	19-45	32	21-47	30.5
0.3	No. 50	8-24	17	(5-17)	11	14-28	17.2
0.075	No. 200	4-12	9	(2-8)	5	5-15	2.3

Table 3: Asphalt Binder Properties

Test	ASTM designation	Test results	SCRB specification
Penetration at [25 °C,100 g, 5 sec]	D5	45	40-50
Ductility [35 °C. 5 cm/min]	D113	113	>100
Softening Point, [°C]	D36	55	---
Flash Point, [°C]	D92	294	>232
Fire Point, [°C]	D92	307	---
Specific Gravity of Asphalt [-]	D72	1.035	---
Rotational Viscometer [Pa. sec]	D4402	0.481@ 135	---
		0.122 @165	---
Loss on Heating [5 hrs at 163 °C]	D1754	0.27%	<0.75
Solubility in trichloroethylene [%]		99.73	99

2.5. Asphalt Concrete Layer

The HMA wearing surface met the Iraqi specifications for wearing courses, using a nominal aggregate size of 19 mm. The amount of asphalt utilized was 4.8%. As shown in Table 4, typical HMA mix characteristics included a maximum specific gravity of 2.57, stability of 10.10 kN, voids in the total mix (VTM) of 4.1%, and voids in mineral aggregate (VMA) of 15.5%. Soundness testing was conducted on the aggregate particles used in the wearing course and base course layer according to ASTM C 88-99, which is a durability test that evaluates aggregate resistance against weathering action, specifically the aggregate resistance to withstand wetting and drying cycle or freezing and thawing conditions. The aggregate is immersed in a saturated solution of magnesium sulphate ($MgSO_4$), followed by oven drying. The loss in weight after five cycles represents the degree of deterioration.

The percent loss for aggregate use in base course was 0.0705% while for wearing course was 0.121, both values within the specification where the maximum acceptable limit is 18% according ASTM specifications.

Table 4: Bituminous Base Course and Wearing Course Mix Properties

Properties	Base		Wearing course	
	Result	Specification	Result	Specification
Asphalt Percent (40-50) Penetration	3.7 [%]	3.0 - 5.5	4.8	4.0-6.0
Stability [kN]	9.4	Min. 5	10.10	Min. 8
Flow [mm]	3.1	2 – 4	3.3	2 – 4
VTM [%]	4.1	3 – 6	4.1	3 – 5
VMA [%]	14.4	-----	15.5	-----
VFB [%]	71.5	-----	73.5	70-85
Density [g/cm^3]	2.311	-----	2.307	-----
Deleterious Material [%]	1.29	Max. 3 [%]	1.314	Max. 3 [%]
Soundness $MgSo_4$ [%]	0.0705	Max. 18 [%]	0.121	Max. [18 %]

Note:
VTM%: Percent of Air Voids in Total Mix
VMA%: Percent of Voids in Mineral Aggregate in the Mix
VFB%: Percent of Voids Filled with Binder (Asphalt) in the Mix
$MgSo_4$: Magnesium Sulphate

2.6. Geogrid Material

Well-known company “Shandong XiuHe”, for Engineering Materials in China, supplied the geogrid material used in this study. Two types of geogrids were utilized. High-tenacity multifilament polyester yarns are used to make polyester biaxial geogrid, which is then covered with a long-lasting polymer. The PP triaxial geogrid TX150, on the other hand, is produced using longitudinal stretching and extrusion techniques using certain grades of high-density polyethylene. It was constructed with ribs aligned in three directions and a hexagonal form. As a result, the triangle apertures were formed by ribs with rectangular cross sections. The manufacturing company’s specifications for the geogrids utilized in this investigation are shown in Table 5, and Figure 3 shows the geogrid types used.

The geogrids were installed at two locations within the pavement model:

1. In the middle depth of the subbase layer
2. At the subbase – subgrade interface

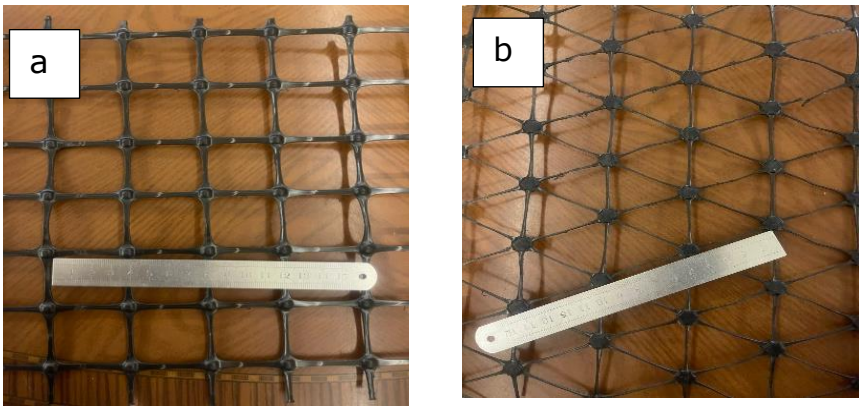

Figure 3: (a) Biaxial Geogrid, (b) Triaxial Geogrid

Table 5: Specifications of PP Biaxial Geogrid (BX3030) and PP Triaxial Geogrid (TX150)

Item	Test Method	Unit	PPX3030		TX150
			MD	TD	
Polymer	-	-	PP	PP	PP
Type			Knitted coated with a durable polymer		Extrude geogrid longitudinal stretch PP fiber
Minimum Carbon Black	ASTM D 4218	[%]	2		2
Aperture Size		[mm]	36	36	40 * 40 * 35
Tensile Strength	ASTM D 6637	[kN/m]	30	30	-
Tensile Strength @ 2% Strain	ASTM D 6637	[kN/m]	10.5	10.5	-
Tensile Strength @ 5% Strain	ASTM D 6637	[kN/m]	21	21	-
Radial Secant Stiffness at 2% Strain	ASTM D 6637	[kN/m]	-	-	185
Elongation	ASTM D 6637	[%]	13	13	13
Junction Efficiency	GRI GG2	[%]	93	93	96
Flexural Rigidity	ASTM D 7748	[mg-cm]	2,000,000		-
Aperture Stability	ASTM D 7864	[m-N/deg]	0.75		-
Roll Width	-	[m]	3.95		3.95
Roll Length	-	[m]	50		50

Notes
MD = Machine Direction; TD = Transverse Direction
PP = Polyethylene

3. Pavement Model Design and Construction

3.1. Experimental Setup and Scaled Models

In this work, the structural reaction of a flexible pavement under repetitive axle loads was simulated using a 1/3 physical scale model. The full-scale pavement prototype chosen from the structural design for Iraqi Express No. 1 has a wearing surface of 4 cm, a binder course of 8 cm, a bituminous base of 20 cm, a subbase of 25 cm, and a subgrade thickness of 150 cm. Layers of 5.0 cm asphalt, 6.0 cm bituminous base, 9.0 cm subbase, and 50.0 cm subgrade made up the comparable scaled model, which had a total thickness of 70 cm.

A rubber tire with an exterior diameter of 30.5 cm was used to represent the load applied for the tests. The prototype of a half single axle load with dual tire 40 KN was reduced to an equivalent load of 5 KN according to (1/3) scale to preserve similar pavement response across the laboratory model and the full-scale pavement. A 3.0 kW hydraulic actuator was used to apply the load with a frequency of 0.21 Hz. This frequency is suitable for pavement response investigation since high-speed results in a reduction in critical pavement response, as the asphalt mixture becomes stiffer at higher frequencies (Jing R. et al., 2020; Garg N. & Gordon F.H., 2001). To examine other scenarios representing moderate pressure and high pressure, the load of 5 KN (480 KPa) was altered to achieve varied pressures. The loads were increased to 6.5 KN and 7.5 KN, which corresponded to pressures of 560 KPa and 690 KPa, respectively, which are measured actual contact pressure.

3.2. Tire Pressure Simulation Setup

An accelerated load test assembly with pneumatic actuators and a rigid tire traveling in a unidirectional path that applied different contact pressures depending on the applied load from 400 kPa to 800 kPa was used to simulate tire pressure using a mechanical load frame, as depicted in Figure 4. This range represents the pressures found in typical commercial vehicles. The color-spray approach was used to experimentally estimate the actual tire–pavement contact area under the scaled load. To replicate actual tire-pavement interaction, the load contact area was computed as an equivalent rectangle in accordance with (Huang Y. H., 2004) and had dimensions of 8.5*12.3 cm, 8.9*13 cm, and 8.7*12.6 cm for 480 kPa, 560 kPa, and 690 kPa, respectively. The loading configuration was created to replicate traffic-induced stress cycles by allowing for repeated loading at regulated pressures.

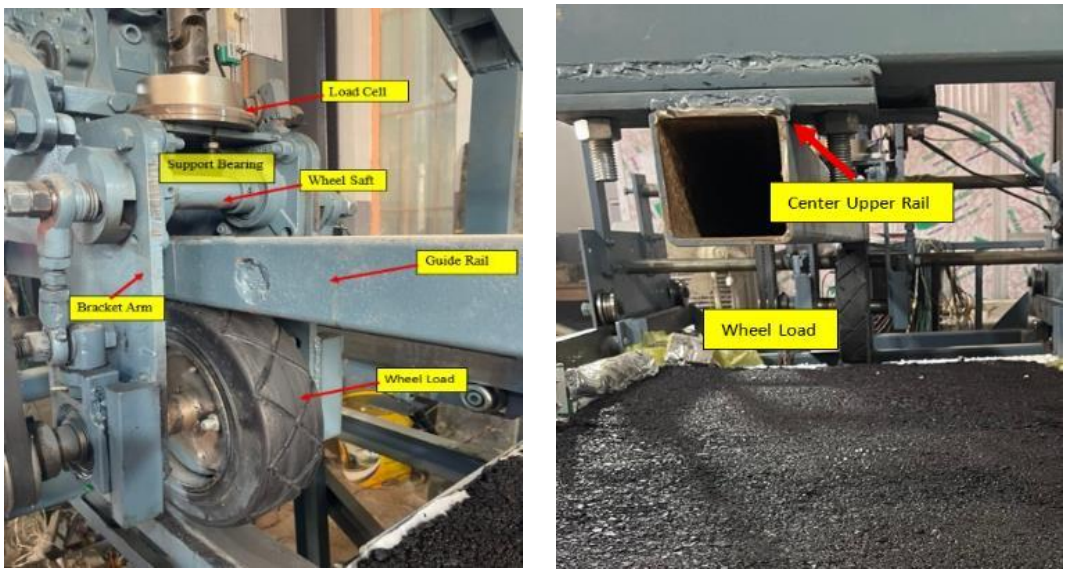

Figure 4: Loading Set up

3.3. Construction of the Scaled Model of Flexible Pavement

The scaled pavement models were built in layers within a strong steel test box that measured 2.0 meters in length, 1.0 meters in width, and 0.70 meters in depth. To prevent the desired moisture content loss, a layer of nylon sheet was placed inside the container, and silicone was applied to the metal box's joint before pavement layers placement. Based on the findings of laboratory compaction, each material layer was carefully prepared and compacted to the desired density and moisture content. The subgrade soil was compacted in successive lifts to achieve a target CBR value of 2.1%, thereby replicating weak subgrade conditions. The initial lift, with a thickness of 10 cm, was compacted manually using a hand tamper. The subsequent second and third lifts, each 20 cm thick, were compacted with a Robin Plate Compactor EY20, featuring a net weight of 100 kg, a 5.0 HP engine, and a Vibration Frequency of around 5800 VPM (vibrations per minute). This compactor is commonly employed for asphalt, soil, sand, gravel, and mixed soils in civil and road engineering applications, as illustrated in Figure 5.

A 3 cm-thick cork layer was mounted at the sides and on the bottom of the box under the subgrade to attenuate wave reflection from the lower base of the rigid metal box and to create a realistic boundary condition. Most geotechnical studies usually use memory foam in a range of thicknesses of (2-2.5) cm. Since memory foam was not available during model construction, a 3 cm thickness of cork was used. The subbase, bituminous base courses, and bituminous wearing course were constructed and compacted to the specified density in a single layer, with thicknesses of 9.0 cm, 6.0 cm, and 5.0 cm, respectively, using the same plate vibratory compactor. For the reinforced sections, biaxial and triaxial geogrids were placed at the middle depth of the subbase layer and at the subbase-subgrade interface during construction. The pavement models of test sections are listed in Table 6.

Table 6: Pavement Test Sections

Section	Type of Geosynthetics	Location of Geosynthetics
Section 1	Non	Control
Section 2	Triaxial Geogrid	Middle of Subbase Thickness [mm]
Section 3	Triaxial Geogrid	Subbase- Subgrade Interface [mm]
Section 4	Biaxial Geogrid	Middle of Subbase Thickness [mm]
Section 5	Biaxial Geogrid	Subbase- Subgrade Interface [mm]

Figure 5: Test Section Construction

3.4. Instrumentation and Data Collection System

A system of load and pressure cell sensors has been installed to measure the pavement's response to repeated wheel loads. High-precision load pressure cells are placed for vertical loads delivered at the top of the subgrade and at the bottom of the asphalt surface layer. With a frequency of 0.21 Hz and a speed of 4.75 km/h (1.320 m/s), the device can handle about 750 load cycle applications per hour. During each test sequence, real-time load and stress data were acquired every 750 cycles, or roughly every hour, and synced with the loading actuator using the data acquisition system and LabVIEW program.

4. Results and Discussions

The scaled test sections shown in Table 6 were prepared to evaluate the performance of the flexible pavement resting on weak subgrade under varying tire pressure with and without geotextile reinforcement. All sections were subjected to identical loading conditions (5, 6.5, and 7.5) KN and tire pressure of (480, 560, and 690) kPa, which represent low, moderate, and high tire pressure, respectively. The performance indicators measured were vertical stress at the bottom of the asphalt surface, vertical stress at the top of the subgrade layer for 25000 load cycles at (45 ± 2) ℃.

4.1. Vertical Stress at the Bottom of the Asphalt Layer

The vertical stress at the bottom of the asphalt wearing course is presented in Figure 6. It can be seen that vertical stress increases with increasing loading cycle, load, and tire contact pressure magnitude in all five test sections. Vertical stress accumulated at a slow rate for the first 5000 cycles, then remained almost at a steady state through the rest loading cycle. This could be attributed to the densification of the surface and Base asphalt layers under the applied load. Table 7 displayed the variation in the percent increase in vertical stress value at different contact tire pressures. Section 1 (control) showed the highest sensitivity with 31.1 % and 27.3 % for pressure rise from (480 to 560) kPa and (650 to 690) kPa, respectively. Recording a total increase of 67% from (480 to 690) kPa in tire pressure.

On the other hand, section 3, which is reinforced with the triaxial geogrid at the subbase-subgrade interface, exhibits the lowest overall section with 47.5%, indicating lower sensitivity to tire contact pressure. At all reinforced sections, there is a notably consistent percentage change through the pavement test sections, with minimum heterogeneity. These results could reflect the variety in load distribution mechanisms due to the type and location of geogrid reinforcement. These results are well aligned with (Jasim A., et al. 2021; AL-Qadi and Wang, 2011; Marshek K. M., et al., 1986; Hussein, M. et al, 2021; Sami, D. A., et al., 2024) who all stated that vertical stress increases with the increase of load cycle and pressure.

Table 7: Maximum Vertical Stress at the Bottom of the Asphalt Layer, kPa

Sections	Description	Tire Pressure [Kpa]			[%] Increase in Vertical Stress		
		480	560	690	[%] Increase from 480 to 560 [kPa]	[%] Increase from 650 to 690 [kPa]	[%] Increase from 480 to 690 [kPa]
Section 1	Control	366.75	480.908	612.403	31.1	27.3	67.0
Section 2	TG in the Middle of the Subbase Layer	318.138	399.512	501.955	25.6	25.6	57.8
Section 3	TG at Subbase-Subgrade Interface	282.177	344.467	416.12	22.1	20.8	47.5
Section 4	BG in the Middle of the Subbase Layer	350.62	435.727	530.141	24.3	21.7	51.2
Section 5	BG at Subbase-Subgrade Interface	293.316	359.386	459.031	22.5	27.7	56.5
Average % for Reinforced Section					25.12 [%]	24.62 [%]	56.0 [%]

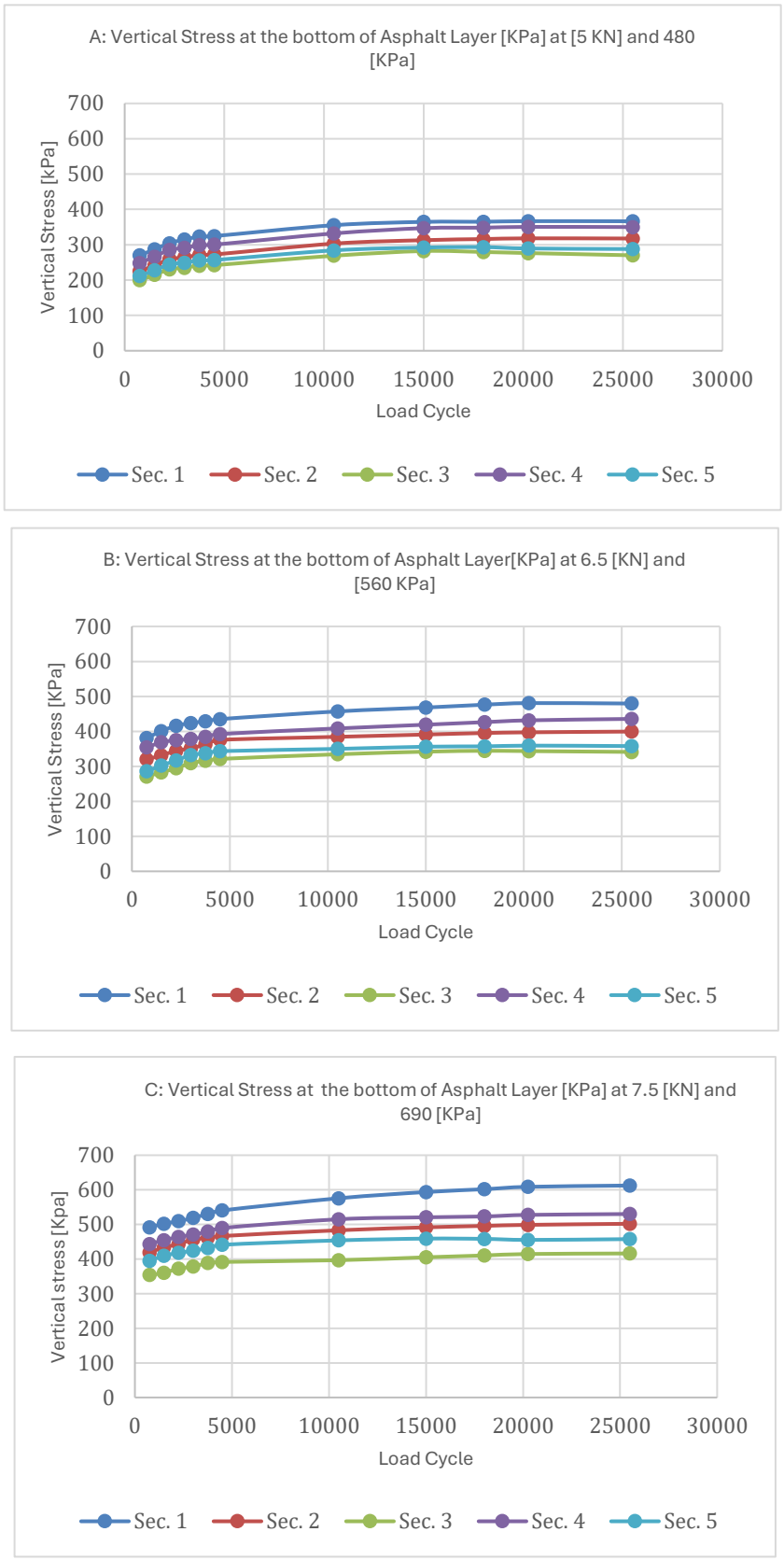

Figure 6: Vertical Stress at the Bottom of Asphalt Surface Layer A: 480 [kPa] Tire Pressure, B: 560 [kPa] Tire Pressure, C: 690 [kPa] Tire Pressure

4.2. Vertical Stress at the Top of Subgrade

Figure 7 shows the vertical stresses at the top of the subgrade, which were measured directly beneath the wheel load path at three different tire pressures: 480, 560, and 690 kPa. Similarly, as the tire contact pressure rises, stress values rise in all pavement test sections. Furthermore, Figure 7 illustrates that the vertical stress increases gradually through the first 5000 cycles and increases at a steady state towards the end of the cycles. Table 8 displays the average increase in maximum stress to the reinforced sections from 480 to 560 kPa, with 16 % and from 650 to 690 kPa, with 13 % with a total percent for 480 to 690 kPa of 32 %, which implies a remarkable reduction in sensitivity to deformation under pressure. These reveal a potential stiffening for the pavement test section and a better confinement mechanism due to geogrid reinforcement. These results are consistent with (AL-Qadi and Wang, 2011; Roberts, F. L., et al., 1985; Marshek, K. M. et al., 1986). (Bonaquist, R., et al.,1988; Sebaaly, P., and Tabatabaee, N., 1989; Sharbaf, M., & Ghafoori, N., 2021) who all reported increases in vertical stress with elevated tire pressure.

4.3. Effect of Geogrid Reinforcement

A comparison between the mean maximum vertical stress at the bottom of the asphalt layer and at the top of the subgrade, presented in Figures 8 and 9, revealed a clear benefit of geogrid inclusion, regardless of geogrid type, under varying pressure (480, 560, and 690 kPa). The control section (1) continuously showed the highest vertical stress. Triaxial geogrid TG exhibited superior performance when compared to Biaxial geogrid BG; the results showed an overall reduction of 16%, 28%, 9%, and 23% for sections 2, 3, 4, and 5, respectively, for vertical stress at the bottom of the asphalt layer, as shown in Table 9. On the other hand, an overall reduction of 35%, 49%, 38%, and 43% was achieved for vertical stress at the top of the subgrade, as illustrated in Table 10. These results are consistent with the established literature (AL-Qadi and Wang, 2011; Roberts, F. L., et al., 1985; Marshek, K. M. et al., 1986). Bonaquist, R., et al., 1988); Sebaaly, P., and Tabatabaee, N.,1989) indicated higher stress levels with higher tire pressure, while Zornberge, 2011; Jasim, A. F. et al., 2021; Jayalath C. P., 2018; Nazzal M.D., 2007; Abo-Farsakh and Nazzal M.D., 2009; Cuelho, 2017) all documented the effectiveness of geosynthetics in minimizing deformations and improving load distribution of pavement built over weak subgrade. Furthermore, section 3 underwent the highest stress percent reduction of 28% and 49% for stress reduction at the bottom of the asphalt layer and at the top of the subgrade. Among all the location arrangements for reinforcement placement, the subbase-subgrade interface has the most effective performance. although the triaxial geogrid had gained a high percentage for stress mitigation, the biaxial geogrid also achieved a good percentage. This could be attributed to the different properties between biaxial and triaxial geogrid that result in different interlocking mechanisms (Sharbaf, M., & Ghafoori, N., 2021).

Table 8: Maximum Vertical Stress at the Top of Subgrade Layer kPa

Sections	Description	Tire Pressure [Kpa]			[%] Increase in Vertical Stress		
		480	560	690	[%] Increase from 480 to 560 [kPa]	[%] Increase from 650 to 690 [kPa]	[%] Increase from 480 to 690 [kPa]
Section 1	Control	49.11	58.982	69.576	20.1	18.0	41.7
Section 2	TG in the Middle of the Subbase Layer	33.395	38.338	42.163	14.8	10.0	26.3
Section 3	TG at Subbase-Subgrade Interface	26.028	30.081	34.516	15.6	14.7	32.6
Section 4	BG in the Middle of the Subbase Layer	30.939	36.568	41.745	18.2	14.2	34.9
Section 5	BG at Subbase-Subgrade Interface	28.975	33.619	38.267	16.0	13.8	32.1
Average Max Reduction [%] for Reinforced Section					16 [%]	13 [%]	32 [%]

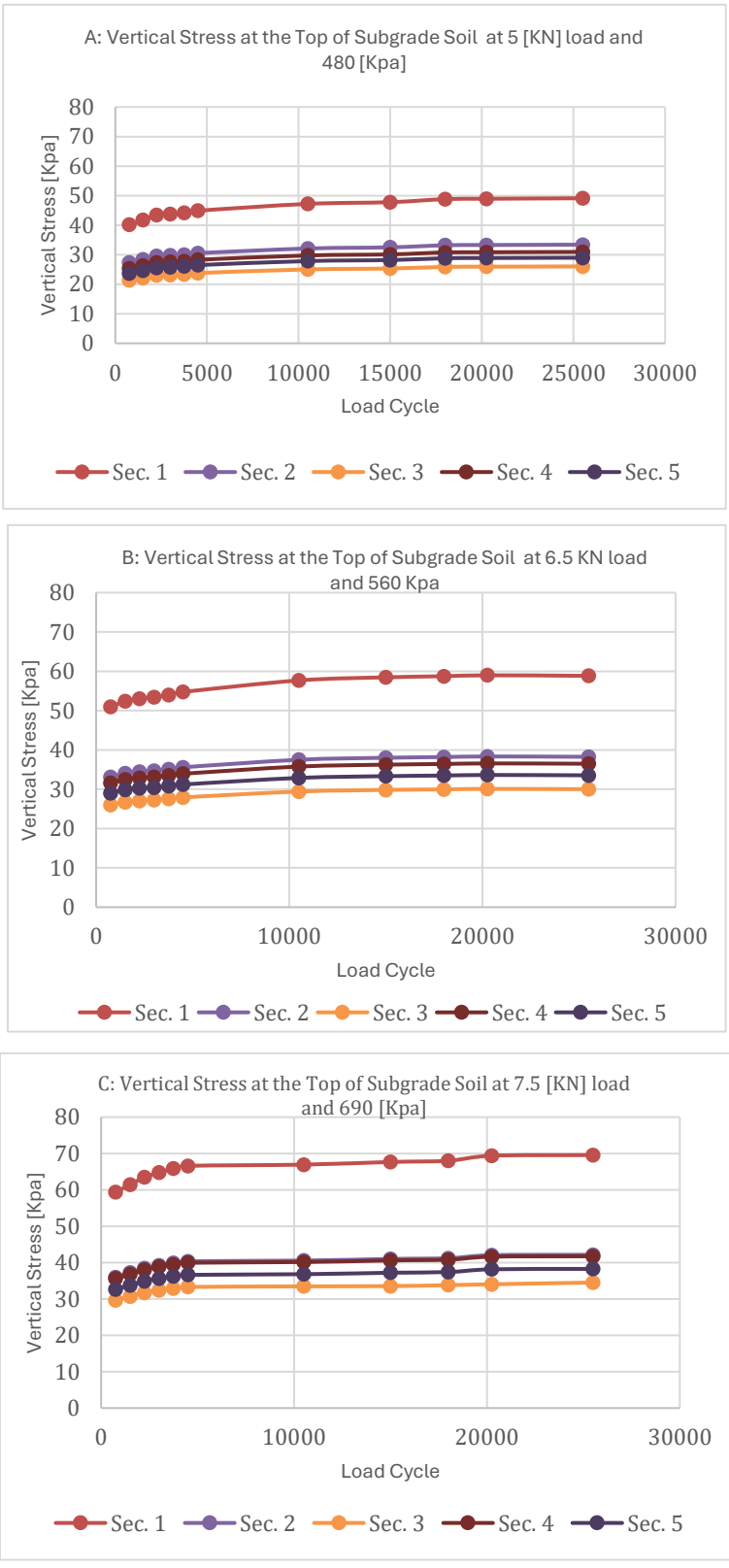

Figure 7: Vertical Stress at the Top of Subgrade Layer A: 480 [Kpa] tire pressure, B: 560 [Kpa] tire pressure, C: 690 [KP] tire pressure

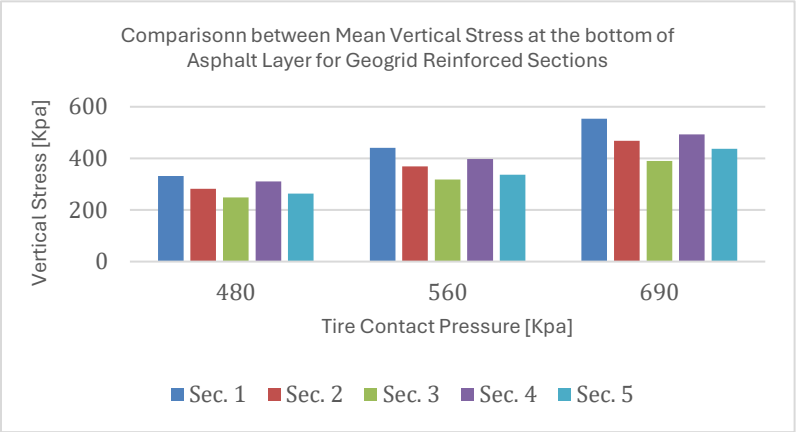

Figure 8: Comparison between Mean Vertical Stress @ the bottom of the Asphalt Layer for Geogrid Reinforced Sections

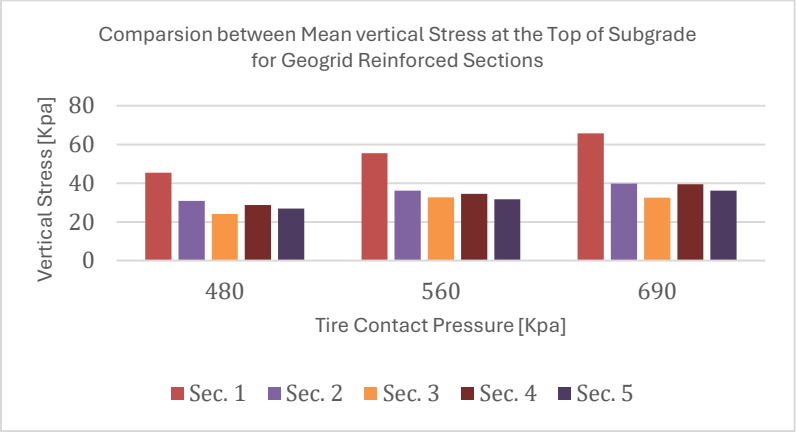

Figure 9: Comparison between Mean Vertical Stress @ the Top of Subgrade for Geogrid Reinforced Sections

Table 9: Stress Reduction Percent for Stress at the Bottom of the Asphalt Layer

Sections	% Mean Stress Reduction due to Reinforcement			Average
	from 480 to 560	from 650 to 690	from 480 to 690	
Sec.1	****	****	****	***
Sec. 2	-13	-17	-18	-16
Sec. 3	-23	-28	-32	-28
Sec.4	-4	-9	-13	-9
Sec. 5	-20	-25	-25	-23

Table 10: Stress Reduction Percent for Stress at the Top of Subgrade Soil

Sections	% Mean Stress Reduction due to Reinforcement			Average
	from 480 to 560	from 650 to 690	from 480 to 690	
Sec.1	****	****	****	***
Sec. 2	-32	-35	-39	-35
Sec. 3	-47	-49	-50	-49
Sec.4	-37	-38	-40	-38
Sec. 5	-41	-43	-45	-43

5. Conclusions

This study investigates the structural reaction of scaled models of flexible pavements, reinforced with geogrid, under varying tire pressures over weak subgrade conditions for flexible pavement model of 5 cm wearing course, 6 cm bituminous base course, 9 cm subbase course all rested on 50 cm clay weak subgrade with 2.1 % CBR. Geogrid reinforcement placed at different position ether in the middle of base layer or at the subbase-subgrade interface. The model of pavement simulates an actual expressway design with high traffic volume constructed over a weak subgrade. The following are the key conclusions based on the material used and the experimental work conducted for the current research:

1. Tire contact pressure significantly affects the stress responses of flexible pavements, with higher pressures (690 kPa) producing up to 67 % higher stresses at the bottom of the asphalt layer for the control section and 56% for the reinforced sections, and up to 42% higher stresses at the top of the subgrade for control and 32 % for reinforced sections when compared to the lowest pressure (480 kPa).

2. Geogrid reinforcement utilization significantly reduces vertical stress at the top of the subgrade layer for flexible pavement over a weak subgrade, with an average percent of 35 % and 49 % for sections reinforced with triaxial geogrid and with a percent of 38 % and 43 % for biaxial reinforced sections, depending on geogrid location.

3. Geogrid reinforcement utilization significantly reduces vertical stress at the bottom of the asphalt layer for flexible pavement over a weak subgrade, with an average percent of 16 % and 28 % for sections reinforced with triaxial geogrid and with a percent of 23 % for biaxial geogrid reinforced sections, depending on geogrid location.

4. Geogrid reinforcement placement at the subbase-subgrade interface has much better performance than placement at the middle of the subbase course.

5. Using a triaxial geogrid at the subbase-subgrade interface reduces the vertical stress at the bottom of the asphalt layer by 28%, while using a biaxial geogrid reduces the vertical stress by 23%.

6. Using a biaxial geogrid at the middle depth of the subbase course reduces the vertical stress at the bottom of the asphalt layer by 9.0 %, while using a triaxial geogrid reduces the vertical stress by 16 %.

7. Using a biaxial geogrid at the subbase-subgrade interface reduces the vertical stress at the top of the subgrade layer by 43%, while using a triaxial geogrid reduces the vertical stress by 49%.

8. Using a triaxial geogrid at the middle depth of the subbase course reduces the vertical stress at the top of the subgrade layer by 35%, while using a biaxial geogrid reduces the vertical stress by 38%

Recommendation

Based on the experimental results of this study, using a triaxial geogrid at the subbase-subgrade interface is highly recommended for flexible pavement reinforcement constructed over weak subgrade at high temperature, especially those expected to encounter high and over contact load pressure. The results have direct significance related to pavement structural design in areas with weak subgrade and overloaded axle weights, which can be incorporated in design guidelines to improve pavement design practice and durability.

Future work should be performed to validate the experimental results by conducting full-scale studies. Studies are needed to investigate the effect of different geogrid types, stiffness, aperture size, and may consider multi-layer reinforcement, or reinforce another type of flexible pavement with a different kind of wearing course, such as polymer-modified mixtures, RAP mixtures, or warm mixtures. In addition, finite element analysis may be considered for a better understanding of the response of flexible pavement under different loading and environmental conditions.

Limitations

The results of this study are valid for the tested geogrid, aggregate, and other materials used. The results may vary if different aggregates and geogrids are used from another source.

Acknowledgements

The author gratefully acknowledges the support provided by the College of Civil Engineering, University of Technology-Iraq, for facilitating the experimental work and providing the laboratory resources. Sincere appreciation is extended to the supervisor, Prof. Dr. Hasan H. J. for valuable guidance and constructive suggestions throughout the research.

Author Contributions

H.H.J. designed the study and supervised the project. **N.D.S.** conducted the experiments and performed the data analysis. Both authors contributed to manuscript writing and critically reviewed and approved the final version of the manuscript and agreed to be accountable for all aspects of the work.

Disclosure of Interest

The authors declare that they have no known competing financial interests or personal relationships that could have appeared to influence the work reported in this paper.

Data Availability Statement

The data supporting the findings of this study are available from the corresponding author upon reasonable request.

References

ASTM D1883-21. (2021). *Standard test method for CBR (California bearing ratio) of laboratory-compacted soils*. ASTM International. https://doi.org/10.1520/D1883-21

ASTM C88 / C88M-18. (2018). *Standard Test Method for Soundness of Aggregates by Use of Sodium Sulfate or Magnesium Sulfate*. ASTM International. https://doi.org/10.1520/C0088_C0088M-1

Abu-Farsakh, Murad, and Munir Nazzal. Evaluation of the base/subgrade soil under repeated loading: phase I-laboratory testing and numerical modeling of geogrid reinforced bases in flexible pavement. No. FHWA/LA. 09/450. Louisiana Transportation Research Center, 2009.

Akram, H. A., Hilal, M. M., & Fattah, M. Y. (2022). Numerical simulation of the effect of repeated load and temperature on the behavior of asphalt layers. *Engineering and Technology Journal*, *40*(5), 1-10.

Al-Qadi, I. L., & Wang, H. (2011). Prediction of tire pavement contact stresses and analysis of asphalt pavement responses: A decoupled approach. Asphalt Paving Technology-Proceedings Association of Asphalt Technologists, 80, 289.

Al-Qadi, I. L., Yoo, P. J., Elseifi, M. A., Janajreh, I., Chehab, G., & Collop, A. (2005). Effects of tire configurations on pavement damage. Journal of the Association of Asphalt Paving Technologists, 74(1), 921-961.

Albayati, A., & Al-Mosawe, H. (2023). Influence of Different Factors on Permanent Deformation of Hot Asphalt Concrete Mixtures. *Civil and Environmental Engineering*, *19*(2), 555-567. https://doi.org/10.2478/cee-2023-0050

Alhelyani, A., & Zhang, S. (2023). Permanent Deformation Evaluation of Modified Asphaltic Pavement Based on Numerical Simulation Models. *Civil and Environmental Engineering*, *19*(1), 178-189. https://doi.org/10.2478/cee-2023-0016

Alimohammadi, H., Schaefer, V. R., Zheng, J., & Li, H. (2021). Performance evaluation of geosynthetic reinforced flexible pavement: a review of full-scale field studies. International Journal of Pavement Research and Technology, 14(1), 30-42. https://doi.org/10.1007/s42947-020-0019-y

Bonaquist, R., Churilla, C., & Freund, D. (1988). Effect of load, tire pressure, and tire type on flexible pavement response. Public Roads, 52(1), 1-7.

Cuelho, E. V., & Perkins, S. W. (2017). Geosynthetic subgrade stabilization – Field testing and design method calibration. Transportation Geotechnics, 10, 22-34. https://doi.org/10.1016/j.trgeo.2016.10.002

Decký, M., Remišová, E., Mečár, M., Bartuška, L., Lizbetin, J., & Drevený, I. (2015). In situ determination of load bearing capacity of soils on the airfields. *Procedia Earth and Planetary Science*, *15*, 11-18.

Garg, N., & Hayhoe, G. F. (2001). Asphalt concrete strain responses at high loads and low speeds at the national airport pavement test facility (NAPTF). In Advancing airfield pavements (pp. 1-14). https://doi.org/10.1061/40579(271)1

Gunasekara Jayalath, C. P., Gallage, C., Dhanasekar, M., Dareeju, B., Ramanujam, J., & Lee, J. (2018). Pavement model tests to investigate the effects of geogrid as subgrade reinforcement. In Proceedings of the 12th Australian and New Zealand young geotechnical professionals conference (pp. 1-8). Australian Geomechanics Society.

Huang, Y. H. (2004). *Pavement analysis and design* (Vol. 2, pp. 401-409). Upper Saddle River, NJ: Pearson/Prentice Hall.

Hussein, M., Fattah, M., & Hilal, M. (2021). Dynamic behavior of pavement layers on sand subgrade. Engineering and Technology Journal, 39(12), 1760-1770. https://doi.org/10.30684/etj.v39i12.1770

Ibrahim, Saad F., Namir G. Ahmed, and Dhuha E. Mohammed. Effect of reinforcement on improve surface pavement for weak subgrade conditions. GEOMATE Journal, 11(23), 2188-2193 (2016).

Jasim, A. F., Fattah, M. Y., Al-Saadi, I. F., & Abbas, A. S. (2021). Geogrid reinforcement optimal location under different tire contact stress assumptions. International Journal of Pavement Research and Technology, 14(3), 357-365.

Jayalath, C., Gallage, C., Wimalasena, K., Lee, J., & Ramanujam, J. (2021). Performance of composite geogrid reinforced unpaved pavements under cyclic loading. Construction and Building Materials, 304, 124570. https://doi.org/10.1016/j.conbuildmat.2021.124570

Jebur, F. F., Fattah, M. Y., & Abduljabbar, A. S. (2021). Function and application of geogrid in flexible pavement under dynamic load. Engineering and Technology Journal, 39(08), 1231-1241.

Jing, R., Varveri, A., Liu, X., Scarpas, A., & Erkens, S. (2020). Study on the asphalt pavement response in the accelerated pavement testing facility. In Proceedings of the 9th International Conference on Maintenance and Rehabilitation of *Pavements—Mairepav9* (pp. 871-880). Springer International Publishing. https://doi.org/10.1007/978-3-030-48679-2_81

Kwon, J., Kim, M., & Tutumluer, E. (2005). *Interface Modeling for Mechanistic Analysis of Geogrid Reinforced Flexible Pavements*. 1–15. https://doi.org/10.1061/40776(155)21

Marshek, K. M., Chen, H. H., Connell, R. B., & Saraf, C. L. (1986). Effect of truck tire inflation pressure and axle load on flexible and rigid pavement performance. Transportation Research Record, 1070, 14-21.

Nazzal, M. D. (2007). Laboratory characterization and numerical modeling of geogrid reinforced bases in flexible pavements. Louisiana State University and Agricultural & Mechanical College.

Rahman, S., Ahmed, A., & Erlingsson, S. (2025). Responses of a thin flexible pavement loaded with tires of various dimensions and configurations. *Road Materials and Pavement Design*, *26*(sup1), 680-699.

Roberts, F. L., Tielking, J. T., Middleton, D., Lytton, R. L., & Tseng, K. (1985). Effects of tire pressures on flexible pavements. Final Report. No. FHWA/TX-86/372-1F.

Sami, D. A., Hameed, H., & Hilal, M. M. (2024). Effect of reinforced asphalt pavement layers with geotextile under dynamic load. In AIP Conference Proceedings (Vol. 3105, No. 1, p. 050063). AIP Publishing LLC. https://doi.org/10.1063/5.0212903

Sebaaly, P., & Tabatabaee, N. (1989). Effect of tire pressure and type on response of flexible pavement. Transportation Research Record, 1227, 92-127.

Sharbaf, M., & Ghafoori, N. (2021). Laboratory evaluation of geogrid-reinforced flexible pavements. Transportation Engineering, 4, 100070.

SCRB, R9, 2003. General Specifications for Roads and Bridges, Department of Planning and Studies, Republic of Iraq, Ministry of Housing and Construction.

Tasnim, S., Shaikh, F. U. A., Sarker, P., Doh, S. I., & Albtoosh, J. F. A. A. (2021). A Comprehensive Review of Flexible Pavement Failures, Improvement Methods and Its Disadvantages. Key Engineering Materials, 879, 136-148.

Wimalasena, K., & Jayalath, C. P. G. (2020). Effect of geogrid reinforcement in weak subgrades. International Journal of Geomate, 18(65), 140–146. https://doi.org/10.21660/2020.65.90377

Zadehmohamad, M., Luo, N., Abu-Farsakh, M., & Voyiadjis, G. Z. (2022). Evaluating long-term benefits of geosynthetics in flexible pavements built over weak subgrades by finite element and Mechanistic-Empirical analyses. Geotextiles and Geomembranes, 50(3), 455–469. https://doi.org/10.1016/j.geotexmem.2022.01.004

Zornberg, J. G. (2015). Advances in the use of geosynthetics in pavement projects. In Keynote lecture, proceedings of the 2nd iberic conference on geosynthetics, Geosintec Iberia (pp. 07-08).

How to Cite This Article

Salman, D. N., & Joni, H. H. (2026). Effects of Geogrid Reinforcement and Tire Contact Pressure on Responses of Flexible Pavement over Weak Subgrade. Civil and Environmental Engineering, 0 (0). https://doi.org/10.2478/cee-2026-0081